ESRF	**Experiment title:** Vectorial magnetic imaging with coherent hard X-rays	**Experiment number**: **MI-1371**
Beamline: ID10	**Date of experiment**: from: February 19th, 2021 to: February 25th, 2021	**Date of report**: March 5th 2021
Shifts: 32	**Local contact(s)**: Federico Zontone, Yuriy Chushkin	*Received at ESRF:*

Names and affiliations of applicants (* indicates experimentalists):

***Guillaume BEUTIER**

Marc VERDIER

Frédéric LIVET

Marisel DI PIETRO

***Alexis WARTELLE**

Report:

Objectives

This beamtime's goals were on one hand the validation of the diamond phase plate recently installed at ID10 to serve as X-ray polarizer, and on the other hand the measurement of Fourier Transform Holography (FTH) on a Fe/Gd microdisk with sensitivity to the three components of magnetization.
The polarizer operates similarly to the X-ray phase retarder implemented by Logan and coworkers [1], by adjusting the diamond plate's tilt with respect to the incident beam around the (2-20) reflection in transmission Bragg geometry. In this way, the beam's polarization can be continuously varied from linear horizontal to linear vertical through circular. Since opposite angular deviations from the ideal Bragg conditions lead to opposite polarization ellipticities, circular left and circular right polarized X-rays can be achieved at the proper polarizer tilts, therefore enabling X-ray Magnetic Circular Dichroism (XMCD) measurements.
In order to test the polarizer's performance, a FTH experiment was designed based on a *ca.* 200-nm-thick Fe/Gd multilayer system which hosts perpendicular magnetic maze domains at zero applied field. A very similar sample has been investigated with hard X-rays by Donnelly and coworkers [2]. For FTH to be possible, the sample fabrication in our case included post-deposition patterning using Focused Ion Beam (FIB): the isolated object to be studied was a 2-µm-diameter disk, and the reference objects were two orthogonal narrow stripes. This particular choice is motivated by the possibilities offered by the Holography with Extended Reference by Autocorrelation Linear Differential Operator (HERALDO) [3]. In this scheme, adequate post-processing allows holographic imaging without the need for high-quality pointlike sources, which are challenging to fabricate and provide little contrast. Stripes are on the other hand easier to produce, and in HERALDO only the sharpness of their tips as well as a narrow width are important for imaging.

Sample fabrication

Fe/Gd multilayer

The multilayer was grown by repeating 150 times the deposition of a bilayer consisting of 4.5 Å of Fe and 9.6 Å of Gd. This leads to an average composition of 43.2 at.% of Gd, and about 211 nm thickness. The process was carried out using an RF magnetron sputtering machine at Institut Néel. The substrate was a Si_3N_4 membrane also provided by Institut Néel.

As far as the patterning is concerned, two strategies were implemented. Both result in an isolated Fe/Gd disk with a diameter of 2 µm, and two orthogonal thin stripes a few µm away to perform HERALDO. The schemes differ in the stripe composition, not in their geometry.

In the first strategy, the three objects are patterned from the Fe/Gd multilayer into a disk with 20 µm diameter where all Fe/Gd has been removed, except at the disk of interest and at the stripes. The design is schematically represented in Fig.1.

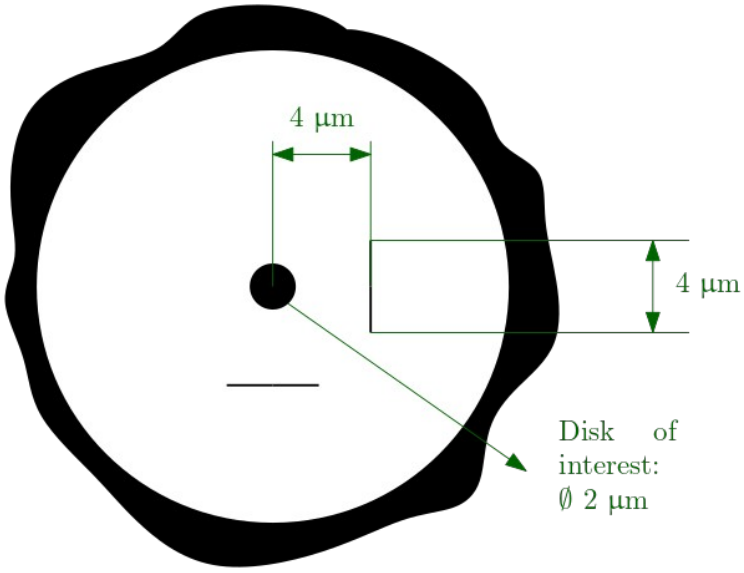

Fig. 1: Schematic design of the sample design for HERALDO. All the Fe/Gd (in black) has been removed from the white area.

The second strategy is similar to the first one, except that in a first step, all the Fe/Gd except the central disk is removed with FIB, then the reference stripes are patterned using a combination of Focused-Ion-Beam-Induced Deposition (FIBID) of Pt and FIB thinning. In this way, relatively wide FIBID-Pt stripes are narrowed down to about 200 nm width, while retaining a vertical aspect ratio slightly above 1. This is illustrated by the Scanning Electron Microscope (SEM) imaging in Fig.2.

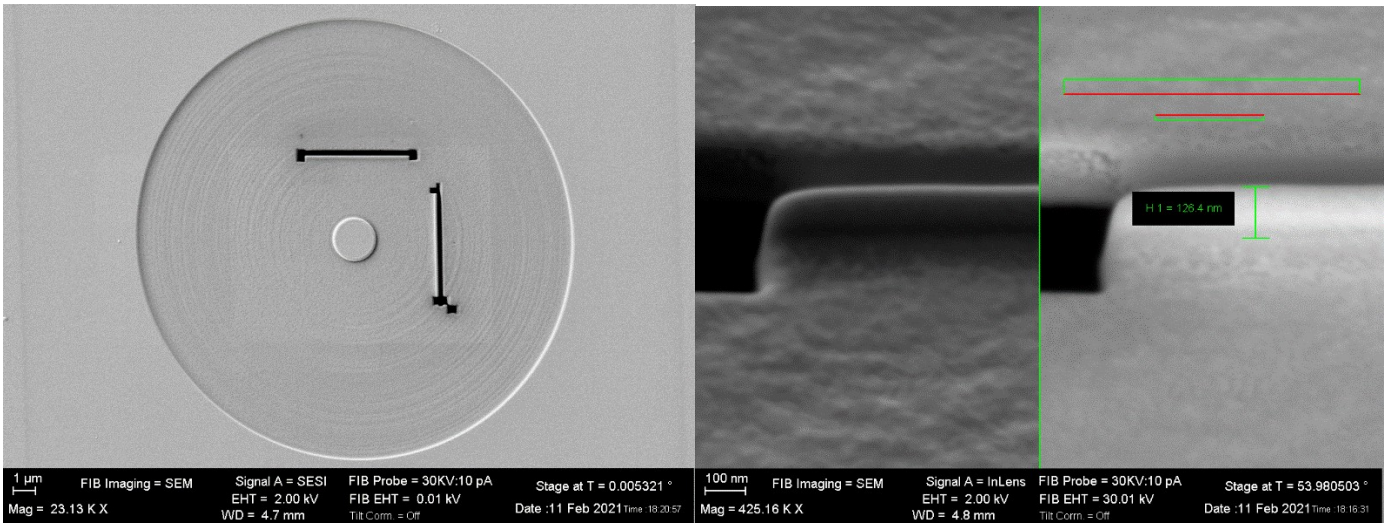

Fig.2: SEM images of the patterned sample following strategy 2. Left: overview. Right: zoom-in on one FIBID-Pt stripe.

In the end, the system depicted in Fig.2 could be completed but not the one corresponding to strategy 1 due to the limited availability of FIB and time constraints. It must be noted that a full thin film (without any pattern) on Si_3N_4 with identical characteristics was prepared and brought for the beamtime. In the following, the patterned sample will be referred to as Beutier 16, the unpatterned multilayer Beutier 17.

Gd:$Nd_2Fe_{14}B$ thick film

A second type of sample was prepared as back-up. This was a 1 µm-thick $Nd_2Fe_{14}B$ film doped with Gd on a thermally oxidized silicon wafer. The composition of this sample, named N2692, was as follows:
Si\SiO_2 (100 nm)\Ta (100 nm)\Gd:$Nd_2Fe_{14}B$ (1 µm)\Ta (10 nm)

The doping was produced by co-depositing $Nd_2Fe_{14}B$ and Gd using triode sputtering. To that end, a piece of Gd was fixed to the $Nd_2Fe_{14}B$ target and the substrate was held stationary in order to create a composition gradient across the wafer. Magnetometry measurements using the Magneto-Optical Kerr Effect (MOKE) were performed at Institut Néel to determine regions with significant coercivity and remanence, indicating a film composition suitable for sizeable out-of-plane magnetization under zero applied field. Thus, such a film is suitable for a direct XMCD measurement in transmission, with the beam perpendicular to the sample. A piece from the composition-graded wafer was therefore cleaved out at the corresponding position. This sample is from here on referred to as N2692_5. Its Gd content was estimated to be *ca.* 5 at.%.
Due to the large thickness of the substrate (*ca.* 300 µm), the transmission experiment was impossible after cleaving. That is why laser drilling was carried out; thanks to previous calibrations, it was possible to thin down the substrate to presumably a few tens of micrometers, over a disk with *ca*. 1.7 mm diameter.

Experimental results

Spectroscopy

First of all, we performed X-ray Absorption Spectroscopy (XAS) on a thin (*ca.* 5 µm thick) Gd foil to confirm the position of the Gd L_3 peak, around which we worked throughout the beamtime. Fig.3 captures several XAS spectra that we acquired on our samples:

- Gd foil (black), from a direct transmission measurement,
- Sample Beutier 17 (red and blue) thanks to the intensity integrated over distinct Regions of Interest (ROIs) from two different energy scans in Small-Angle X-ray Scattering (SAXS),
- N2692_5 (green) from a direct transmission measurement.

It must be noted that the data from Fig.3 has been normalized to a measure of the incident flux, then each curve was offset and multiplied by a constant to present them on the graph in a readable manner.
While the Gd foil and the Gd:$Nd_2Fe_{14}B$ sample do show the L_3 edge at the expected photon energy of 7243 eV [4], we note a shift in the case of the Fe\Gd multilayer system. We do not have an explanation for the significant and abrupt drop in post-edge absorption (at about 7.265 keV) in the Gd:$Nd_2Fe_{14}B$ sample.

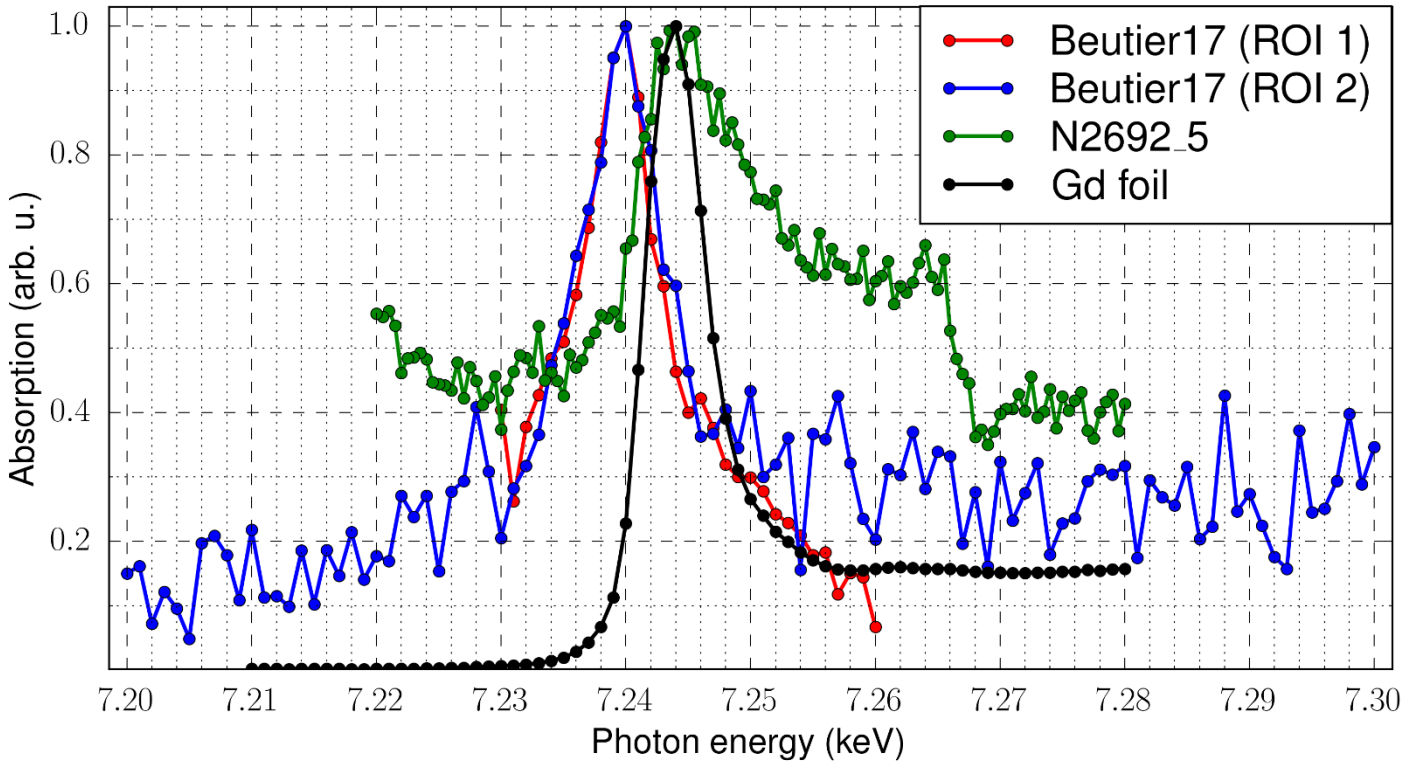

Fig. 3: XAS spectra from our samples Beutier 17, N2692_5, and a Gd foil as reference

Polarizer

In order to monitor the polarization state of our X-ray beam, we used two photomultiplier detectors: one in the storage ring plane, one exactly above the beam. Both detectors were equipped with pinholes (~1 mm size at about 15 cm from the beam), therefore, considering their position, their signal were therefore proportional to the number of σ- and π-polarized photons, respectively.

As stated above, the polarization state is modified by rotating the diamond phase plate. A typical scan in the rotation stage's angle around the diamond Bragg peak results in curves such as depicted in Fig.4; they are in good agreement with what has been reported in the literature [1].

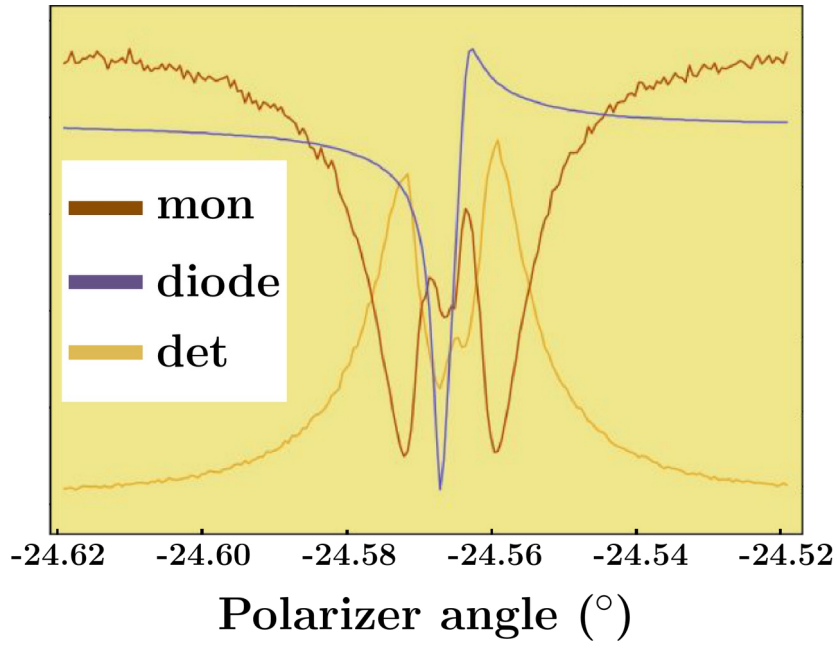

Fig.4: Scan of the polarizer angle across the Bragg peak used for polarization control. "det" and "mon" are the above-mentioned photomultiplier detectors, while "diode" is a measure of the transmitted intensity.

Under the assumption of ideal and perfectly balanced detectors, the angular positions at which circular polarization can be achieved correspond to equal photon counts on the detectors “mon” and “det”. In the following, we will label a measurement as performed under circular polarization if this equality has been (approximately) reached beforehand, though we note that it does not warrant pure circular polarization.

Due to dispersion, these positions must be searched for at any photon energy of interest. In principle, this could even be tabulated. However, we have found the system diamond plate plus rotation stage not reliable enough. To be more precise: working it only in very small steps (as is required for our study) leads to a degradation of performance over time. This can be clearly observed as jumps during angular scans and a rougher and rougher curve aspect. An example is provided in Fig.5, which shows the det and mon signals of two consecutive angular scans; jumps are indicated by the blue arrows.

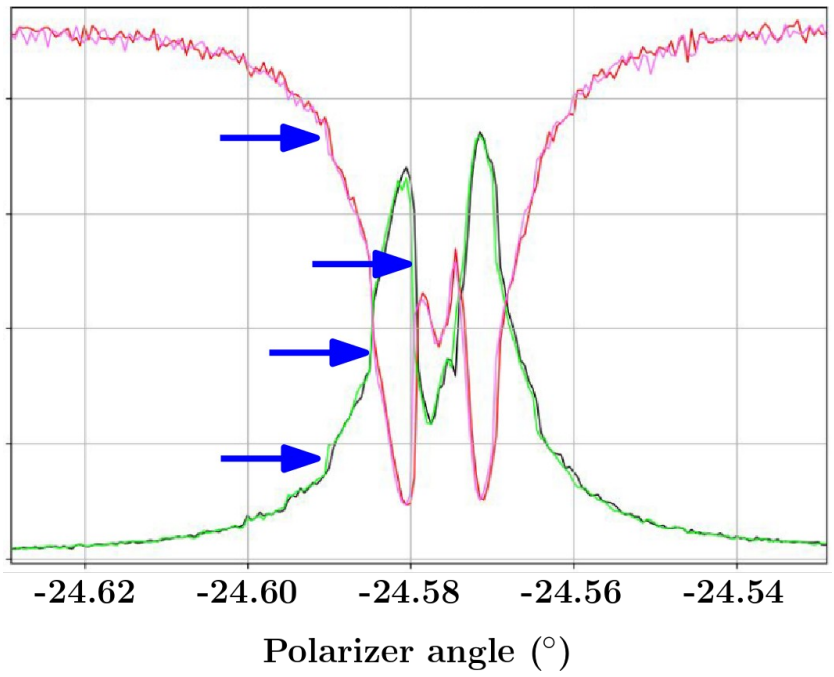

Fig.5: det (pink, red) and mon (green, black) signals during two consecutive, identical polarizer angle scans. Jumps are clearly seen, cf. blue arrows.

Over time, it became clear that the rotation stage’s tolerance (in terms of absolute position) and motion velocity also played a role in the polarizer’s performance. It must be noted that the angular position does not seem to drift over time, as we could confirm from very stable det and mon photon counts if the rotation stage stands still. It is the motion that becomes problematic over time; in some cases, not even the characteristic double-peak shape from Figs.4-5 can be recognized.

On the positive side, we received feedback from the company (SmarAct) which sold the rotation stage. Since the stage’s design is compatible with our *in vacuo* operating conditions, their opinion is that the issues are linked to the operation in very small steps. This flushes the motor’s lubricant away from the working positions, leading to performance degradation. And indeed, rotating the stage by even 1° and back improves the scan qualities. Furthermore, it was recommended to make the device perform calibrations every now and then, and this also allowed to recover a smooth, jump-free behaviour as depicted in Fig.4.

As a conclusion, we did succeed in operating the diamond plate as a polarizer; we can nearly extinguish the photon counts on either σ or π detector and obtain linear vertical resp. horizontal polarization. Based on the careful detetector design, we assume that circular polarization is achieved when both detectors receive the same flux, which we can easily accomplish within a couple percents either manually or algorithmically. Nevertheless, care must be taken during operation to regularly restore the rotation stage’s performance through device calibration or deliberate large excursions.

As discussed above, the measurement protocol for this sample was that of a transmission XMCD experiment. The intensity of the direct beam transmitted through the sample was derived from the current flowing through a photodiode serving as detector. This is the "diode" that is mentioned in Fig.4. Additionnally, in the place where the sample was thinned down with laser drilling, two-dimensional maps could be obtained by scanning the sample across the beam.

Our very first attempt consisted in measuring the diode with circularly polarized X-rays of opposite helicities across the Gd L_3 edge at a sample position with near-optimal transmission. Denoting I_+ and I_- are the currents at opposite photon helicities, the corresponding dichroic signal S then reads:

$$S = I_{+¿} - \frac{I_{-¿}}{I_{+¿}+I_{-¿}} ¿$$

Unfortunately, the energy scan was disturbed by poor polarizer behaviour. Without much hindsight at the time, we moved on to acquiring a 2D map of the transmission at a fixed energy and a fixed polarizer angle (corresponding to equal counts on det and mon) before and after rotating the sample by 180° around the vertical axis. Indeed, flipping the sample orientation in this way is equivalent to reversing the photon helicity. Then, the intensities are normalized by the photon flux (measured as mon+det) before the dichroic contrast is computed as in the above equation at every point. The results from this scan are presented in Fig. 6. While the average transmission (left) displays features that do not quite coincide with those from the normalized XMCD image (middle), the presence of XMCD is not obvious; even less so if one considers the right-hand side image, which is computed as an XMCD image, although the starting point is two maps with the same circular polarization and sample orientation. In other words, this image should be exactly zero everywhere. We point out, however, that on the XMCD images, data points such that the transmission was below 20% of its maximum value are not displayed i.e. their XMCD value is set to 0. Furthermore, not removing the zeroes outside the areas with significant transmission, the actual XMCD image features a standard deviation of about $7.1*10^{-3}$, the "false" one $4.7*10^{-3}$. Thus, we may have measured some XMCD barely above the noise level in this case.

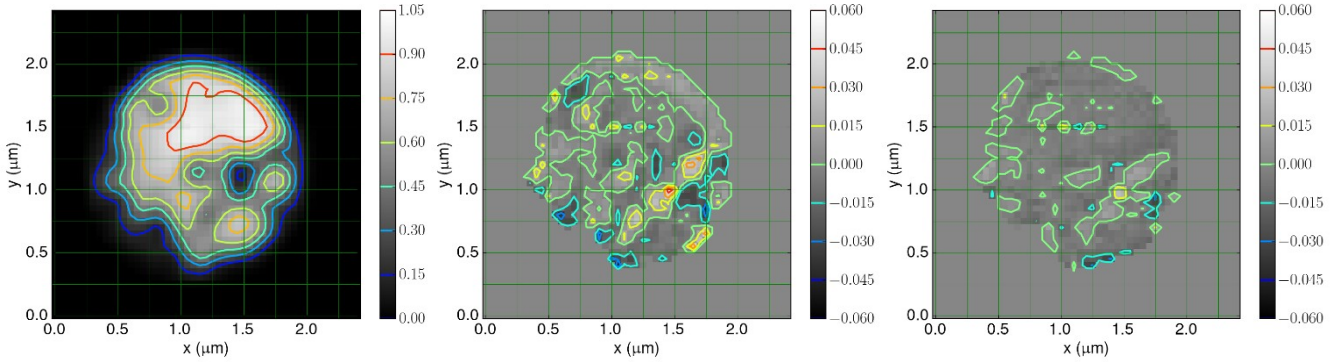

Fig.6: Average transmission (left) through the sample, normalized XMCD (middle) and "false" XMCD computed with two images with the same orientation. Both the middle and right-hand side images were set to zero in places where the total intensity was less than 20% of its maximum value across the 2D map.

After the 2D mapping, we have used a pulsed magnetic field system [5] to apply 4 T to the sample. Our concern was that the laser drilling might have induced a thermal demagnetization. Then, we moved on and recorded the normalized XMCD in transmission (at a fixed position) as a function of photon energy once more. However, the results' signal-to-noise ratio was too weak to draw conclusions. Therefore, we changed sample.

Beutier 16

Unfortunately, we found out that the Si_3N_4 membrane supporting the FIB-patterned disk and FIBID-Pt reference stripes was broken before it was mounted on the sample holder.

Beutier 17

The remanent state for this sample features perpendicular magnetic maze domains. This has been confirmed by Magnetic Force Microscopy (MFM) measurements; the period of the domain pattern is about 1.8 micrometers. In Fig.7, we present on the left side the frequency shift (indicative of out-of-plane stray fields) measured with MFM and on the right side the modulus of the frequency shift's Fourier transform. We note an artifact corresponding to a laterally shifted replica of the maze pattern, which results in a horizontal distortion of the expected ring in Fourier space. Nevertheless, the domain period can be extracted from the ring's extent.

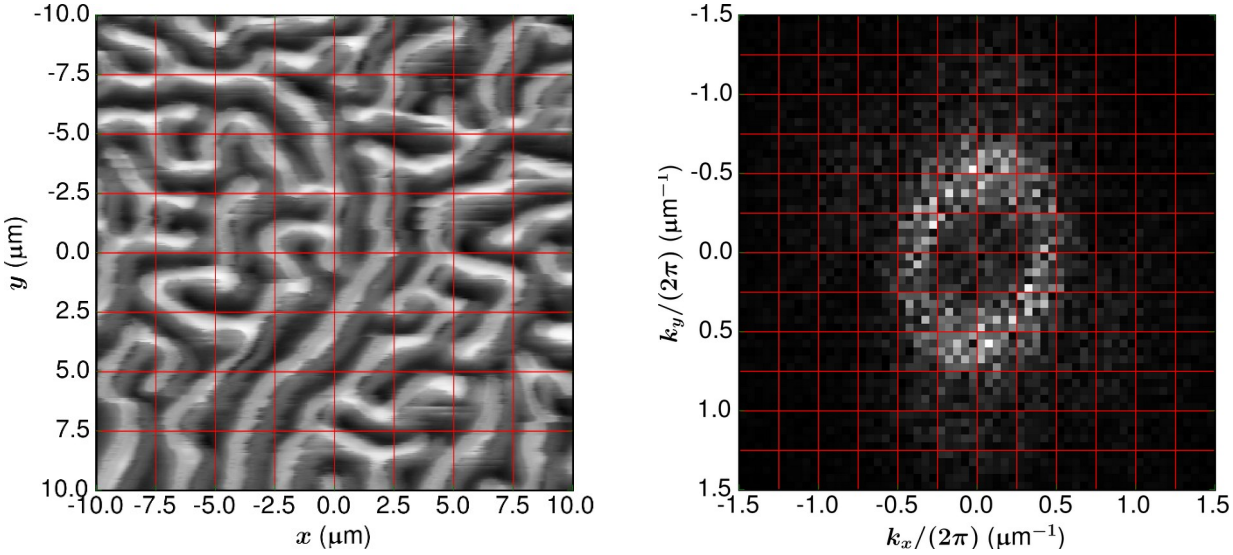

Fig.8: MFM frequency shift (left) on sample Beutier 17, revealing the maze domain pattern (left), and modulus of its Fourier transform (right).

We therefore began to acquire SAXS images using the polarizer so as to measure XMCD speckle patterns. Fig.8 presents one of our first imaging of this kind at a photon energy of 7.239 keV, just below the Gd L_3 edge in this sample (cf Fig.3). We point out that the right-hand side image is a difference image not normalized by the sum of opposite polarization images. This choice is motivated by the fact that normalized differences can appear overly large at low photon counts, whereas regular differences actually weigh XMCD by the statistics and are thus easier to assess. The only normalization performed is the division by the flux measure det+mon.

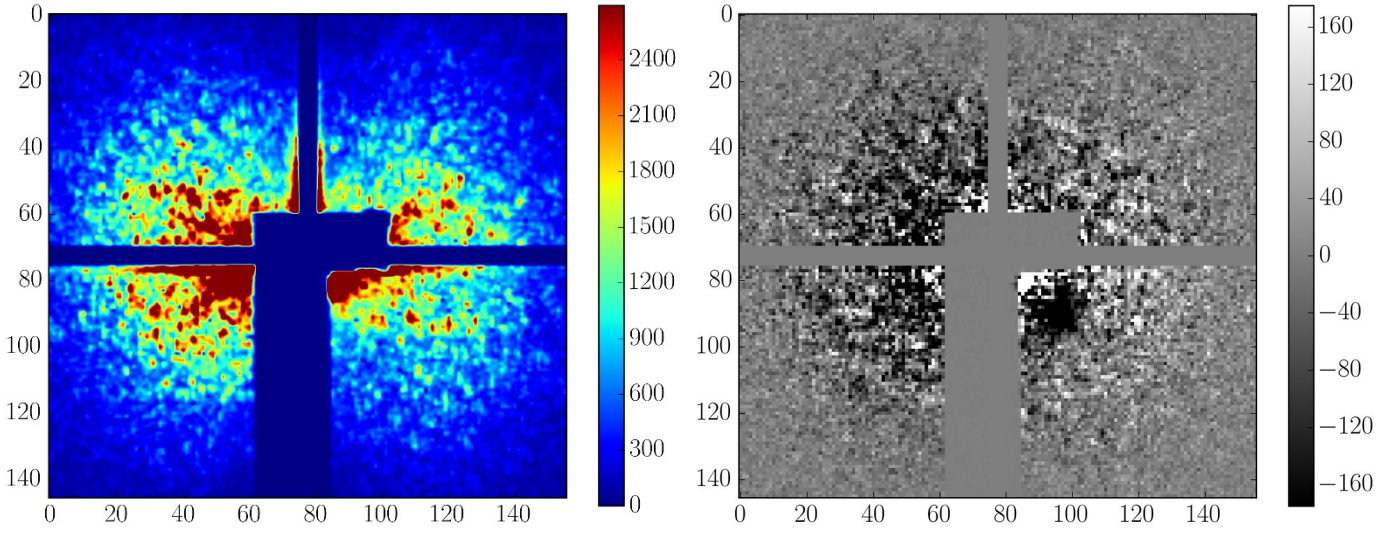

Fig.8: Regular SAXS image from the sample with circular polarization (left) and difference image (right) between two opposite circular polarizations.

Interestingly, the difference pattern does not quite have the same overall shape as the regular SAXS image; moreover, it appears to be bipolar. This is reminiscent of the findings by Chauleau and coworkers [6] on a system that also featured perpendicular magnetic maze domains. It must be noted that the strong feature with negative values at about (90,90) is likely a contribution from a truncation rod due to the finite diamond plate thickness.

Despite this, we recorded difference images across the Gd L_3 edge. We succeeded in implementing a routine to rotate the polarizer to the circular polarization angles, based on guess values far enough below/above the lower/upper intersection mon=det. The intersection is located to within an arbitrary margin.
A few images from the energy scan are displayed in Fig.9. At 7.22 keV i.e. below the absorption edge, the difference signal should be vanishing. On the image, it is not; however, close inspection of the images taken at opposite helicities reveals a slight drift in the whole SAXS pattern. This has of course a dramatic impact on the difference image, which makes it less reliable than, for instance, the following image at 7.235 keV. In this one, no clear dichroic signal is present. By contrast, on-edge at 7.239 keV, we observe a strong bipolar pattern as discussed above. Increasing the photon energy, we persistently observe such a non-centrosymmetric pattern up to 7.244 keV (corresponding image not shown here); its asymmetry and overall strength progressively decrease. Far above the absorption edge, at 7.26 keV, the only clear features left are from the phase plate's truncation rod or direct-beam-related artifacts.

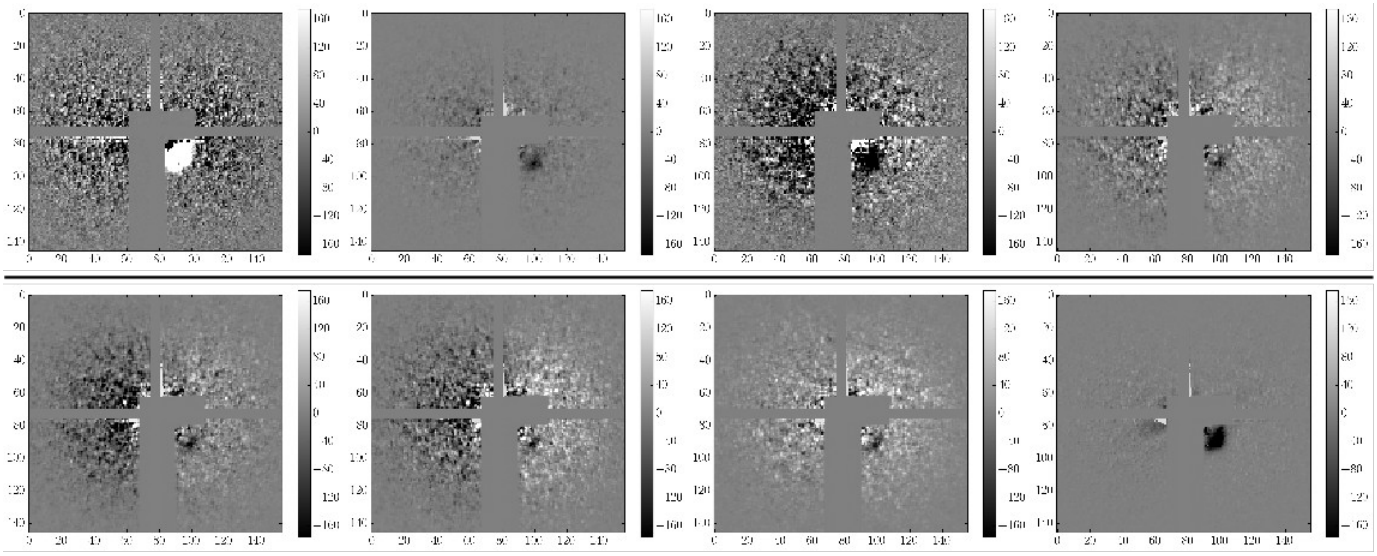

Fig.9: Difference images at different photon energies, given in keV. Top row, from left to right: 7.22, 7.235, 7.239, 7.24. Bottom row, from left to right: 7.241, 7.242, 7.245, 7.26.

In order to quantify this patterns evolution, we plot in Fig.10 the difference signal averaged over the upper left quadrant. This choice results from the fact that this appears to be the quadrant least affected by the truncation rod or other artifacts over the energy range. We took care to reject the beamstop as well as the blind cross from the detector. While we note that no drift correction was performed, and that some artifacts might still be present, Fig.10 displays clear on-edge signal which we attribute to XMCD.
Instead of a single-peak shape, we observe a more complex dispersion. This is not so surprising since our signal corresponds to the scattering pattern of waves undergoing XMCD, as a result, both the real and imaginary parts of the scattering pattern contribute, and their dispersions are starkly different, as is illustrated for instance in reference [2].

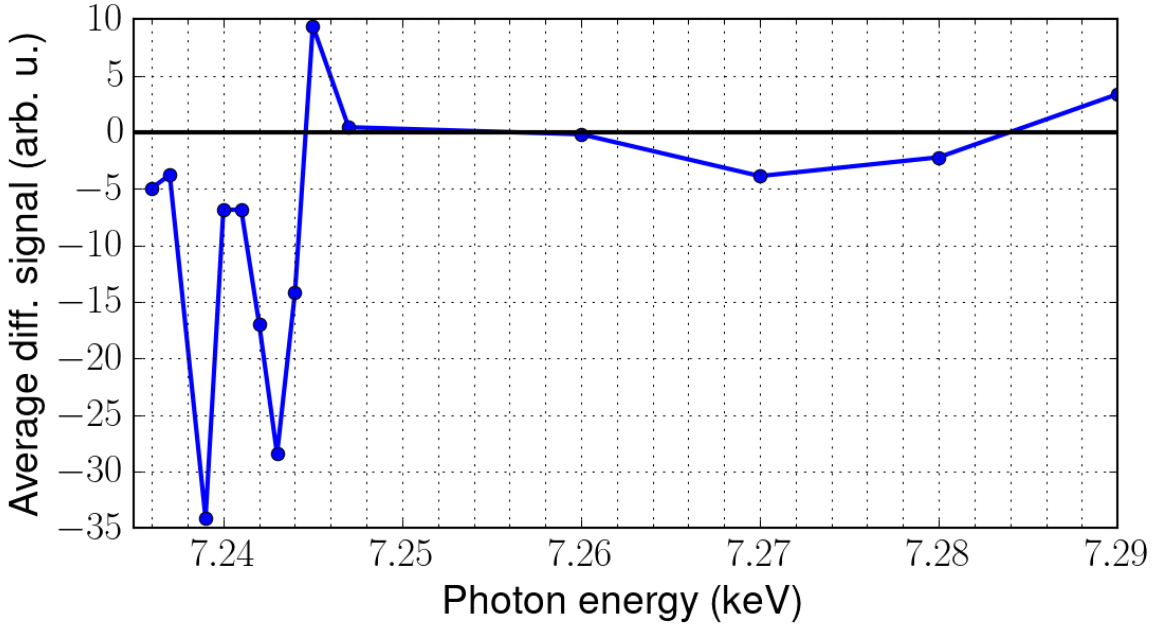

Fig.10: Difference signal averaged over top left quadrant (beamstop and detector blind cross not included), as a function of photon energy.

Our last experiment on this sample consisted in gluing a 5-micrometer-wide pinhole on the backside of the membrane. The idea was to measure strong speckle patterns corresponding to a limited sample area. However, the measured SAXS pattern was seen to persistently drift until the end of our beamtime. It did not stabilize, as could be confirmed by correlation measurements; hence, subsequent acquisitions at different circular polarizations predominantly reflect the pinhole drift instead of XMCD.

References

[1] Logan *et al.,* J. Synchrotron Rad. (2016). **23**, 1210-1215
[2] Donnelly *et al.*, Physical Review B **94**, 064421 (2016)
[3] Guizar-Sicairos and Fienup**,** Opt Express **15**, 26 (2007)
[4] X-ray data booklet, Center for X-ray Optics and Advanced Light Source, Lawrence Berkeley National Laboratory, 2009
[5] PuMag project: https://www.linksium.fr/en/projects/pumag
[6] Chauleau *et al.*, Physical Review Letters **120**, 037202 (2018)